Title

The Old Host-galaxy Environment of SSS17a, the First Electromagnetic Counterpart to a Gravitational-wave Source* * This paper includes data gathered with the 6.5 meter Magellan Telescopes located at Las Campanas Observatory, Chile.

Authors

Pan, Y-C
Kilpatrick, CD
Simon, JD
et al.

The Old Host-galaxy Environment of SSS17a, the First Electromagnetic Counterpart to a Gravitational-wave Source[*]

Y.-C. Pan[1], C. D. Kilpatrick[1], J. D. Simon[2], E. Xhakaj[1], K. Boutsia[3], D. A. Coulter[1], M. R. Drout[2,10], R. J. Foley[1], D. Kasen[4,5], N. Morrell[3], A. Murguia-Berthier[1], D. Osip[3], A. L. Piro[2], J. X. Prochaska[1], E. Ramirez-Ruiz[1,6], A. Rest[7,8], C. Rojas-Bravo[1], B. J. Shappee[2,9,11], and M. R. Siebert[1]

[1] Department of Astronomy and Astrophysics, University of California, Santa Cruz, CA 95064, USA
[2] The Observatories of the Carnegie Institution for Science, 813 Santa Barbara Street, Pasadena, CA 91101, USA
[3] Las Campanas Observatory, Carnegie Observatories, Casilla 601, La Serena, Chile
[4] Nuclear Science Division, Lawrence Berkeley National Laboratory, Berkeley, CA 94720, USA
[5] Departments of Physics and Astronomy, University of California, Berkeley, CA 94720, USA
[6] DARK, Niels Bohr Institute, University of Copenhagen, Blegdamsvej 17, DK-2100 Copenhagen, Denmark
[7] Space Telescope Science Institute, 3700 San Martin Drive, Baltimore, MD 21218, USA
[8] Department of Physics and Astronomy, The Johns Hopkins University, 3400 North Charles Street, Baltimore, MD 21218, USA
[9] Institute for Astronomy, University of Hawaii, 2680 Woodlawn Drive, Honolulu, HI 96822, USA

Abstract

We present an analysis of the host-galaxy environment of Swope Supernova Survey 2017a (SSS17a), the discovery of an electromagnetic counterpart to a gravitational-wave source, GW170817. SSS17a occurred 1.9 kpc (in projection; $10''2$) from the nucleus of NGC 4993, an S0 galaxy at a distance of 40 Mpc. We present a *Hubble Space Telescope* (*HST*) pre-trigger image of NGC 4993, *Magellan* optical spectroscopy of the nucleus of NGC 4993 and the location of SSS17a, and broadband UV-through-IR photometry of NGC 4993. The spectrum and broadband spectral-energy distribution indicate that NGC 4993 has a stellar mass of $\log(M/M_\odot) = 10.49^{+0.08}_{-0.20}$ and star formation rate of $0.003\,M_\odot\,\mathrm{yr}^{-1}$, and the progenitor system of SSS17a likely had an age of >2.8 Gyr. There is no counterpart at the position of SSS17a in the *HST* pre-trigger image, indicating that the progenitor system had an absolute magnitude $M_V > -5.8$ mag. We detect dust lanes extending out to almost the position of SSS17a and >100 likely globular clusters associated with NGC 4993. The offset of SSS17a is similar to many short gamma-ray-burst offsets, and its progenitor system was likely bound to NGC 4993. The environment of SSS17a is consistent with an old progenitor system such as a binary neutron star system.

Key words: galaxies: individual (NGC 4993) – stars: individual (SSS17a)

1. Introduction

On 2017 August 17 (UT), the Laser Interferometer Gravitational-wave Observatory (LIGO) and Virgo interferometer detected a gravitational-wave source from a binary neutron star (BNS) merger, GW170817 (LIGO/Virgo Collaboration 2017b; LIGO Scientific Collaboration and Virgo Collaboration 2017, in preparation). Two seconds after the LIGO/Virgo detection, the *Fermi* Gamma-ray Space Telescope and *INTErnational Gamma-Ray Astrophysics Laboratory* (*INTEGRAL*) detected a short-duration gamma-ray burst (sGRB; INTEGRAL 2017; LIGO/Virgo Collaboration 2017a). About 11 hr after the LIGO/Virgo trigger, our team discovered an optical transient in NGC 4993 coincident with GW170817, called Swope Supernova Survey 2017a (SSS17a; One-Meter Two-Hemisphere (1M2H) Collaboration 2017; Coulter et al. 2017).

SSS17a is the first detection of an electromagnetic counterpart to a gravitational-wave source. This discovery marks a milestone and opens a new era in modern astronomy. The gravitational-wave data suggests that SSS17a is a BNS merger, the most popular progenitor model of sGRBs (e.g., Eichler et al. 1989; Lee & Ramirez-Ruiz 2007; Berger 2014).

The host environments of astrophysical transients have long been a profitable route to understanding the nature of their progenitor systems and placing broad constraints on their properties. For example, the long-duration GRBs and sGRBs have very different host environments. While long GRBs predominantly occur in star-forming galaxies (e.g., Bloom et al. 2002), sGRBs can be found in both star-forming and early-type galaxies (Prochaska et al. 2006; Fong et al. 2013), indicating an older population. In addition, sGRBs tend to be found in more massive galaxies and generally show larger offsets from their hosts than long GRBs do (Zheng & Ramirez-Ruiz 2007; Behroozi et al. 2014). The distinct host properties suggest they are likely to arise from different progenitor populations.

In this work, we investigate the host environment of SSS17a, both globally and locally. By comparing our results to those from different kinds of astrophysical transients, we constrain the nature of the progenitor system.

A plan of the paper follows. In Section 2, we describe the observations and data reduction, and Section 3 discusses the methods used to analyze the data and show the determined host properties. The discussion and conclusions are presented in Sections 4 and 5, respectively. Throughout this paper, we assume $H_0 = 70\ \mathrm{km\ s^{-1}\ Mpc^{-1}}$ and a flat universe with $\Omega_M = 0.3$ when necessary.

2. Observations and Data Reduction

SSS17a was discovered $5\rlap{.}''3$ E and $8\rlap{.}''7$ N of NGC 4993 (1M2H Collaboration 2017; Coulter et al. 2017), an early-type S0 galaxy with redshift $z = 0.009727 \pm 0.000050$ (de Vaucouleurs et al. 1991) in a galaxy group (Makarov & Karachentsev 2011). The transient is only 1.9 kpc offset (projected) from NGC 4993, assuming the distance to NGC 4993 of 39.5 Mpc based on the Tully–Fisher method (Freedman et al. 2001).

NGC 4993 was observed by the *Hubble Space Telescope* (*HST*) with the Advanced Camera for Surveys (ACS) on 2017 April 28 (UT) in the *F606W* filter as part of the "Schedule Gap Pilot" program (Program 14840; PI: Bellini). We obtained the *HST* images from the Mikulski Archive for Space Telescopes. We reduced the *HST* image using the DRIZZLEPAC pipeline (Avila et al. 2015). The calibrated frames were further corrected for geometric distortion, sky background, and cosmic-rays, and combined with ASTRODRIZZLE. We registered the final combined images using TWEAKREG.

We performed photometry on the combined *HST*/ACS image following standard procedures with DOLPHOT.[12] The DOLPHOT photometry was calibrated using the ACS/WFC *F606W* zeropoint for 2017 April 28 from the ACS zeropoint calculator.[13]

We obtained Pan-STARRS1 (PS1) *griz* imaging of NGC 4993 from the PS1 image cutout server[14] (Chambers et al. 2016). These data had been calibrated to the PS1 system following procedures described in Magnier et al. (2016).

To measure the photometry of NGC 4993, we fit an elliptical isophote to the galaxy profile using the IRAF package ISOPHOTE. We measured an *HST*/ACS *F606W* AB magnitude of 12.23 ± 0.01 mag. Using the same method, we measured PS1 *griz* AB magnitudes of 12.45 ± 0.02, 12.14 ± 0.02, 11.78 ± 0.02, and 12.62 ± 0.02 mag, respectively. In addition, we obtained far-UV and near-UV (NUV) photometry from the *Galaxy Evolution Explorer* (*GALEX*; Bianchi et al. 2017), JHK_s near-infrared photometry from the Two Micron All-Sky Survey (2MASS; Skrutskie et al. 2006), and 3.6–22 μm IR photometry from the *Wide-field Infrared Survey Explorer* (Wright et al. 2010).

We examined the position of SSS17a in the *HST*/ACS *F606W* image and did not detect any sources at the transient location. Placing artificial stars on similar surface-brightness areas, we determined an AB magnitude limit at the position of SSS17a of $m_V > 27.2$ mag, corresponding to $M_V > -5.8$ mag at the distance of NGC 4993, consistent with limits initially reported by *HST* (2017).

We obtained an optical spectrum of NGC 4993 on 2017 September 5 (UT) using the $f/4$ camera of the Inamori-*Magellan* Areal Camera and Spectrograph (ImacS; Dressler et al. 2006) on the 6.5 m *Magellan*/Baade telescope at Las Campanas Observatory. We used the $600\,\ell/\text{mm}$ grating with a blaze angle of $8\rlap{.}°6$ to cover the wavelength range 3500–6500 Å at a spectral resolution of $R \approx 2500$. We obtained three 600 s exposures on NGC 4993 with a $0\rlap{.}''7$-wide long slit in mediocre conditions with some clouds. We carried out basic reductions of the spectra (bias subtraction, wavelength calibration, flatfielding, and coaddition) using the COSMOS software

---

package (Dressler et al. 2011).[15] We then extracted the spectrum over a $3\rlap{.}''7$-diameter aperture in IRAF and applied a flux calibration derived from observations of the standard star LTT 6248. The flux-calibrated spectrum of NGC 4993 is displayed in the upper panel of Figure 2.

3. Analysis

3.1. Stellar Mass and Star Formation Rate

We use the photometric redshift code Z-PEG (Le Borgne & Rocca-Volmerange 2002), which is based on the spectral synthesis code PÉGASE.2 (Fioc & Rocca-Volmerange 1997), to estimate the host-galaxy stellar mass (M_{stellar}) and star formation rate (SFR). Z-PEG fits the observed galaxy colors with galaxy SED templates corresponding to nine spectral types (SB, Im, Sd, Sc, Sbc, Sb, Sa, S0, and E). We assume a Salpeter (1955) initial-mass function. The photometry is corrected for foreground Milky Way reddening of $E(B - V) = 0.109$ mag (Schlafly & Finkbeiner 2011; Shappee et al. 2017) with $R_V = 3.1$ and a Cardelli et al. (1989, CCM) reddening law.

Using our 14-band photometry (see Section 2), we measure a host M_{stellar} of $\log(M/M_\odot) = 10.49^{+0.08}_{-0.20}$, corresponding to a halo mass of $\log(M_{\text{halo}}/M_\odot) = 11.96$ using the M_{stellar}–M_{halo} relation derived in Yang et al. (2008), assuming $\log(M_0/M_\odot) = 9.8$, $\log(M_{\text{h}}/M_\odot) = 10.7$, $\alpha = 0.6$ and $\beta = 2.9$ in their Equation (7). The observed photometry and best-fit template can be found in Figure 3.

In Figure 4 we compare the measured M_{stellar} to that for the host galaxies of supernovae (SNe) and both short and long GRBs. Similar to SNe Ia and core-collapse SNe, sGRBs can be found in galaxies with a wide range of M_{stellar}. By contrast, long GRBs are predominantly found in low-mass galaxies. We find that NGC 4993 is more massive than 50% of host galaxies for all classes. In fact, NGC 4993 is more massive than *every* long GRB host galaxy in the Leibler & Berger (2010) sample.

Z-PEG also indicates negligible recent star formation (at least over the past 0.5 Gyr) in the host galaxy. The same result is obtained by intentionally forcing Z-PEG to better fit the UV photometry (but sacrificing the goodness of the full SED fitting; see the gray curve in Figure 3). This is further supported by the non-detection of nebular emission lines in the host spectrum. Using the *GALEX NUV* photometry, we estimate an SFR of only $0.003\ M_\odot\ \text{yr}^{-1}$ (see also VAST 2017) based on the conversion from Kennicutt (1998).

3.2. Age and Metallicity

The spectrum of NGC 4993, through its continuum and possible emission lines, provides information about its extinction, SFR, metallicity, age, and velocity dispersion. To measure these quantities, we fit the emission lines and stellar continuum using the Interactive Data Language (IDL) codes PPXF (Cappellari & Emsellem 2004) and GANDALF (Sarzi et al. 2006). A complete description of this process can be found in Pan et al. (2014). Briefly, PPXF fits the line-of-sight velocity distribution (LOSVD) of the stars in the galaxy in pixel space using a series of stellar templates. Before fitting the stellar continuum, the wavelengths of potential emission lines are masked to remove any possible contamination. The stellar templates are based on the MILES

---

[12] http://americano.dolphinsim.com/dolphot/
[13] https://acszeropoints.stsci.edu/
[14] http://ps1images.stsci.edu/cgi-bin/ps1cutouts

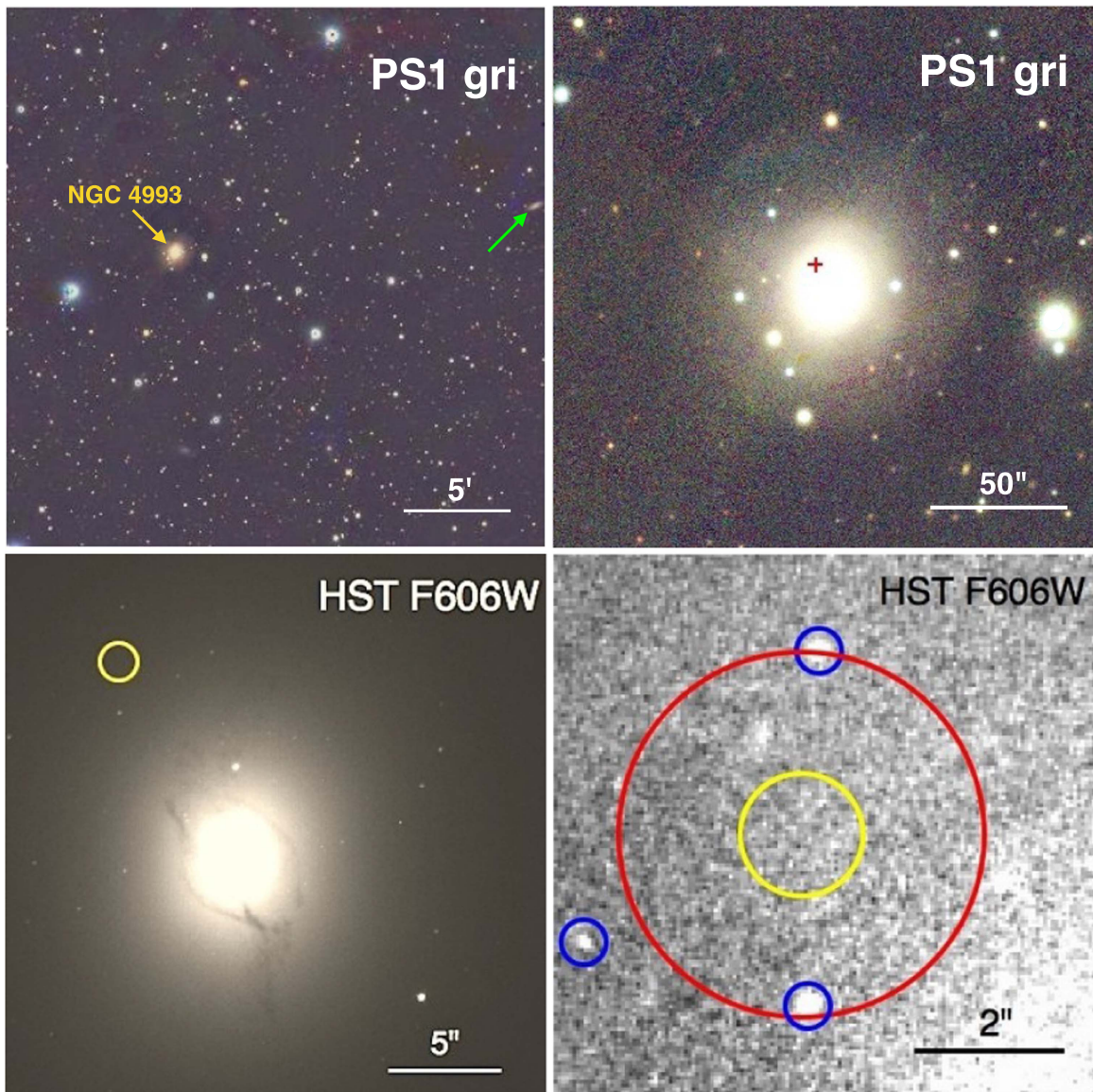[15] http://code.obs.carnegiescience.edu/cosmos

Figure 1. Upper left: false-color (RGB channels corresponding to PS1 *irg* filters) image of the field surrounding NGC 4993 (indicated by the yellow arrow). The green arrow marks the closest galaxy to NGC 4993 in the same galaxy group, ESO 508-G018. Upper right: zoom-in of the upper-left image centered on NGC 4993. The red cross marks the location of SSS17a. Lower left: *HST*/ACS F606W image near the center of NGC 4993. The yellow circle represents the 1-σ error circle of the SSS17a location. The dust lanes surrounding the galactic center are obvious. Lower right: zoom-in of the lower-left image after subtracting a GALFIT model, centered on the SSS17a location. The yellow circle and red circle represent the 1-σ and 3-σ astrometric uncertainty, respectively. Blue circles mark the potential globular clusters near the transient location. For all images, north is up and east is left.

empirical stellar library (Sánchez-Blázquez et al. 2006; Vazdekis et al. 2010). A total of 288 templates are selected with $[M/H] = -1.71$ to $+0.22$ in six bins and ages ranging from 0.063 to 14.12 Gyr in 48 bins.

After measuring the stellar kinematics with PPXF, the emission lines and stellar continuum are fit by GANDALF simultaneously. Through an iterative fitting process, GANDALF finds the optimal combination of the stellar templates, which have already been convolved with the LOSVD. Extinction is handled using a two-component reddening model. The first component assumes a diffusive dust screen throughout the whole galaxy that affects the entire spectrum, including emission lines and the stellar continuum, while the second is a local dust component around the nebular regions, and

therefore affects only the emission lines. The spectral fit results from PPXF and GANDALF can be found in Figure 2.

PPXF determines a heliocentric radial velocity $cz = 2961 \pm 5\,\mathrm{km\,s^{-1}}$ and central velocity dispersion of $161 \pm 8\,\mathrm{km\,s^{-1}}$ for NGC 4993. The best-fit value for the diffusive dust component is zero (the local dust component cannot be constrained due to the lack of nebular emissions in our spectrum), suggesting that dust extinction within the inner $3\rlap{.}''7$ of NGC 4993 is negligible.

In Figure 2 we show the stellar age and metallicity distributions of the host-galaxy stellar populations given by the PPXF fit. We determine a mass-weighted mean stellar age of 10.97 Gyr, with the youngest and oldest stellar populations having ages of 2.8 Gyr and a Hubble time, respectively. This
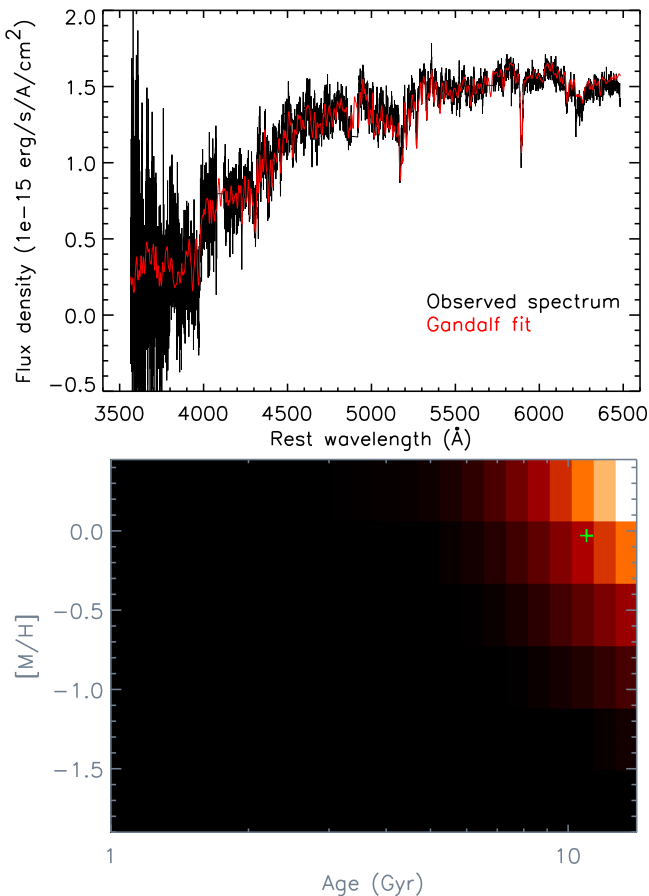
Figure 2. Top: *Magellan*/IMACS spectrum of NGC 4993. The red spectrum shows the spectral fit recovered with the GANDALF software package. Bottom: a grid containing a total of 288 stellar templates (a combination of six metallicities and 48 ages) used for PPXF fitting. Here, we only plot the templates with age older than 1 Gyr. The weight of each template is represented by the strength of the color. The templates with higher weights are brighter. We present here the result for NGC 4993. The green cross represents the weighted mean stellar age and metallicity.
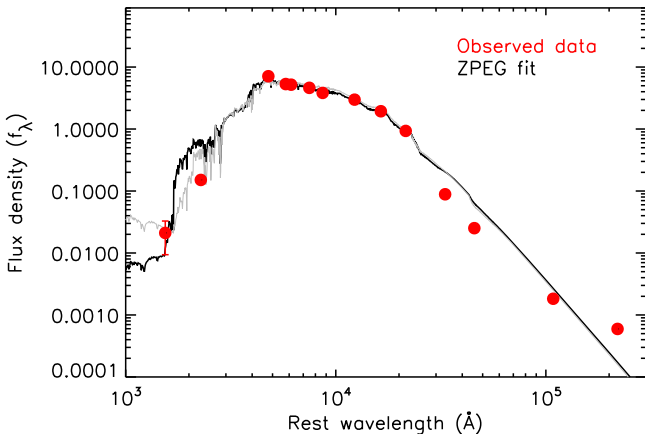
Figure 3. Best-fit SED template by Z-PEG (black curve) to the observed 14-band photometry (red filled circle). The gray curve represents the template by intentionally forcing Z-PEG to better fit the UV photometry but sacrificing the goodness of fitting on other bands.

result strongly suggests that the progenitor system of SSS17a was at least 2.8 Gyr old. Our result is consistent with previous findings that sGRBs tend to originate from older populations (Leibler & Berger 2010).

We measure a mass-weighted mean stellar metallicity $[M/H] = -0.03$, corresponding to $\sim 0.9\,Z_\odot$. Leibler & Berger (2010) used the gas-phase metallicity $12 + \log(O/H)$ and measured a mean metallicity of $\sim 1\,Z_\odot$ for sGRB samples. They also found that the metallicities of sGRB hosts are generally higher than those for long GRB hosts (with a median metallicity of only $\sim 0.3\,Z_\odot$). Therefore, NGC 4993 has a typical metallicity for an sGRB host galaxy.

3.3. Offset and Fractional Flux

SSS17a is offset by $10\rlap{.}{''}2$ from the center of NGC 4993, corresponding to a physical (projected) offset of 1.9 kpc using the Tully–Fisher distance of 39.5 Mpc (Freedman et al. 2001). In Figure 4, we compare the measured offset to that for different types of transients. It is evident that the locations of sGRBs tend to be farther from the centers of their host galaxies (with a median offset of 5 kpc) than long GRBs and other SNe. We find that the offset of SSS17a is somewhat small in comparison to sGRBs, with $\sim 77\%$ of all sGRBs having an offset of >1.9 kpc. This same trend is true when normalizing the offset by the effective radius of the galaxy, where SSS17a has a normalized offset of $r/r_e = 0.61$, and $\sim 80\%$ of all sGRBs have larger normalized offsets.

To further study the local environment of the transient, we use the fractional flux method (e.g., Fruchter et al. 2006). The fractional flux is defined as the sum of all flux in all pixels that are fainter than that measured at the location of the transient divided by the total flux associated with the galaxy. Using the *HST*/ACS $F606W$ image, we determine a fractional flux of 0.41 for SSS17a (Figure 4). With this metric, sGRBs do not trace the optical light of the galaxy, with $\sim 45\%$ of all sGRBs being at positions with effectively no galaxy light. That is, sGRBs are often found in the far outskirts of a galaxy. By contrast, long GRBs tend to be in the brightest part of their host galaxies (with a median fractional flux of 0.86), suggesting that their progenitors are likely related to bright star-forming regions.

The fractional flux of SSS17a is relatively high compared to sGRB samples (~ 80th percentile; consistent with the offset distribution), but low relative to long GRBs (only ~ 4th percentile).

3.4. Morphology

NGC 4993 is clearly an S0 galaxy (Capaccioli et al. 2015). To further quantify its morphology, we use GALFIT (Peng et al. 2002) to fit the surface-brightness profile of NGC 4993. We fit the galaxy profile with a single Sérsic model given by

$$\Sigma(r) = \Sigma_e \exp\{-\kappa[(r/r_e)^{1/n} - 1]\}, \qquad (1)$$

where r_e is the effective radius such that half of the total flux is enclosed within r_e, Σ_e is the surface brightness at the effective radius, r_e, n is the Sérsic index (a concentration parameter), and κ is a variable coupled to n.

Fitting the *HST* image of NGC 4993, GALFIT gives a concentration parameter $n \approx 4$ (the de Vaucouleurs profile), which is similar to typical elliptical galaxies. The effective radius r_e is $17''$, corresponding to a physical size of 3.3 kpc. A residual image is created by subtracting the best-fit model from the original image (see Figure 5).

Dust lanes are clearly seen in the residual image, extending several kpc from the galactic center (see both Figures 1 and 5) roughly in the direction of SSS17a (HST 2017). However, the dust lanes do not appear to reach the position of SSS17a, providing further evidence that SSS17a does not suffer strong
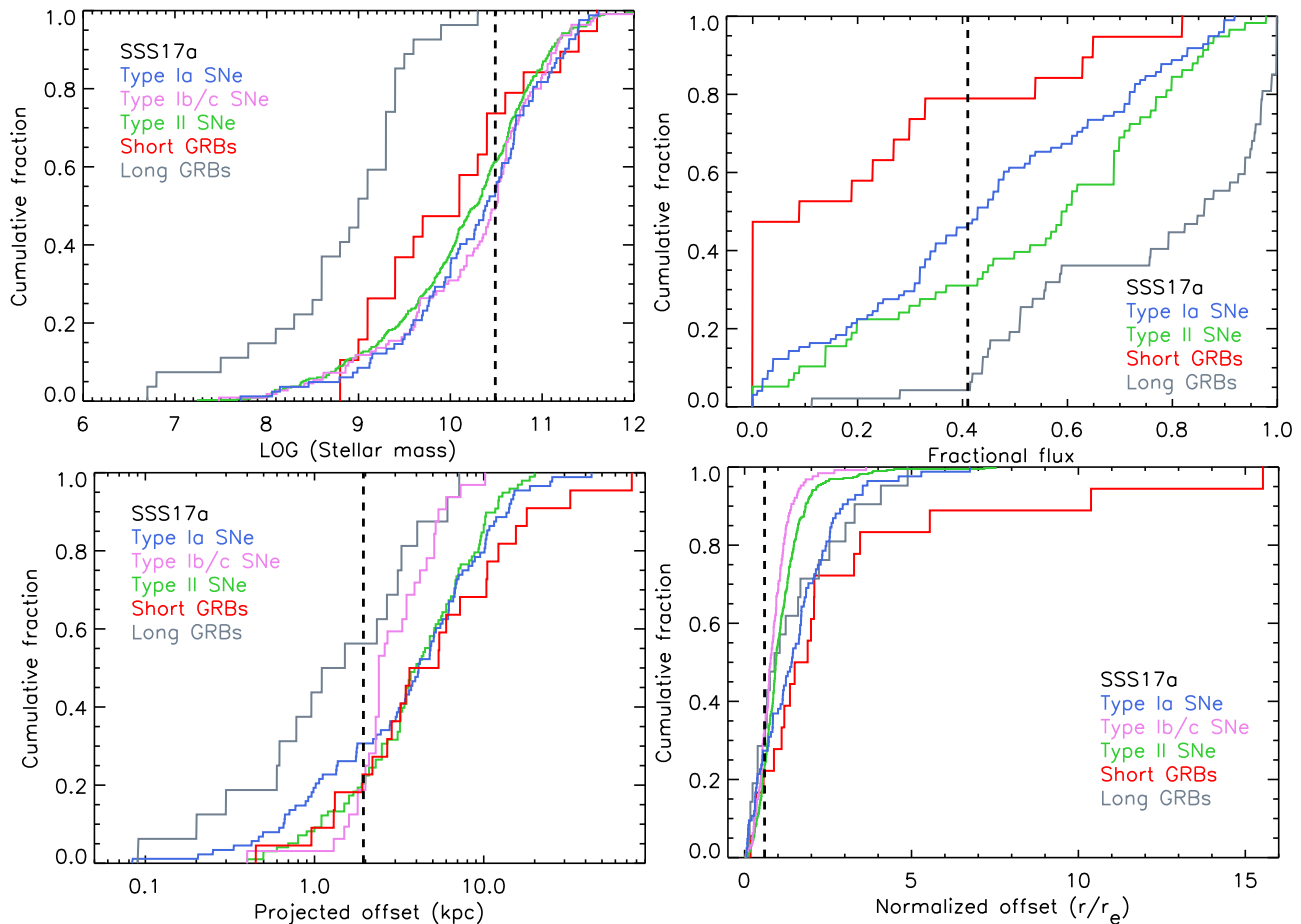
Figure 4. Upper left: cumulative distribution of host-galaxy stellar mass for different classes of transients. The host mass of SSS17a is represented by a vertical dashed line. Also shown are the distributions for SNe Ia (blue; Pan et al. 2014), SNe Ib/c (violet; Kelly & Kirshner 2012), SNe II (green; Kelly & Kirshner 2012), sGRBs (red; Leibler & Berger 2010), and long GRBs (gray; Leibler & Berger 2010). Upper right: same as the upper-left panel, but for the fractional flux. Also shown are the distributions for SNe Ia (Wang et al. 2013), SNe II (Svensson et al. 2010), sGRBs (Fong et al. 2013), and long GRBs from Fruchter et al. (2006) and Svensson et al. (2010). Lower left: same as the upper-left panel, but for the projected offset from the host center. Also shown are the distributions for SNe Ia (Pan et al. 2014), SNe Ib/c (Prieto et al. 2008), SNe II (Prieto et al. 2008), sGRBs (Fong et al. 2013), and long GRBs (Bloom et al. 2002). Lower right: same as the upper-left panel, but for the normalized offset relative to the host effective radius r_e. Also shown are the distributions for SNe Ia (Pan et al. 2014), SNe Ib/c (Kelly & Kirshner 2012), SNe II (Kelly & Kirshner 2012), sGRBs (Fong et al. 2013), and long GRBs (Bloom et al. 2002).

extinction and is consistent with the results of Shappee et al. (2017). The dust lanes found in early-type galaxies are usually indications of recent minor mergers and likely to host active galactic nuclei (Shabala et al. 2012).

3.5. Globular Clusters

Globular clusters contain very high densities of stars. This high stellar density increases the probability of close interactions and leads to mergers more frequently than for field stars (Grindlay et al. 2006; Lee et al. 2010; Samsing et al. 2014). Here we investigate the possibility that SSS17a originated from a globular cluster in NGC 4993.

To better detect sources hidden in the diffuse stellar light, we use the GALFIT residual image (Section 3.4) and identify sources using SEXTRACTOR (Bertin & Arnouts 1996, see Figure 5). To identify possible globular clusters, we require that each source have the following properties: (1) not obviously a foreground star (we cross-check this by using a catalog such as USNO-B1.0), (2) point-like PSF, and (3) a brightness consistent with a globular cluster at 40 Mpc given the globular cluster luminosity function (e.g., Faifer et al. 2011), specifically those with $21 \leqslant m_{AB} \leqslant 24$ mag (corresponding to $-10 \leqslant M_{AB} \leqslant -7$ mag). A total of 119

sources pass these cuts and are selected as potential globular clusters, with the closest one being ~ 290 pc away in projection from the position of SSS17a. In principle, we should be able to detect all of the globular clusters in the image (the detection limit is ~ 27 mag). However, the number estimated here could be underestimated due to the dust extinction or the relatively bright background near the host nucleus.

Previous studies (e.g., Peng et al. 2008) showed that the total mass of globular clusters (M_{GCS}) within the host galaxy can be estimated by a simple scaling relation to the host-galaxy halo mass (M_{halo}) via

$$M_{GCS}/M_{halo} = \eta, \qquad (2)$$

where η represents the absolute efficiency of globular cluster formation. Assuming an efficiency $\eta \simeq 4 \times 10^{-5}$ (Harris et al. 2015) and an average globular cluster mass of $4 \times 10^5 M_\odot$ (Spitler & Forbes 2009), the number of globular clusters (N_{GCS}) within a galaxy of M_{halo} can be estimated by

$$N_{GCS} = (1.0 \times 10^{-10}) \times M_{halo}. \qquad (3)$$

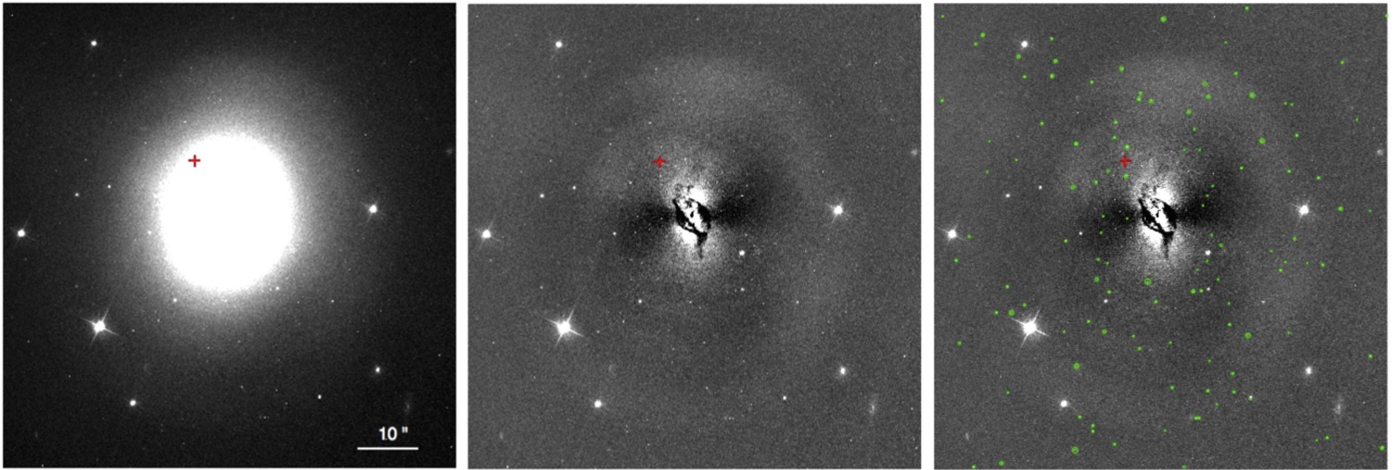Using $N_{GCS} = 119$ (the number of likely globular clusters detected in the HST image), we determine

Figure 5. Left: *HST*/ACS *F*606*W* image of NGC 4993. Middle: residual image created by subtracting a single Sérsic profile modeled by GALFIT from the same image. Right: candidate globular clusters detected (in green) after our cuts described in Section 3.5. The radius of the circle is proportional to size of the source. The red cross in each image represents the location of SSS17a.

$\log(M_{\mathrm{halo}}/M_{\odot}) = 12.07$, which is close to the value that we found using the $M_{\mathrm{stellar}}-M_{\mathrm{halo}}$ relation (see Section 3.1).

4. Discussion

In Section 3.3 we show that sGRBs tend to have larger offsets from their host galaxies than other kinds of transients. The observed offset distribution is generally consistent with the predictions for compact object mergers (e.g., Behroozi et al. 2014). Simulations show that these progenitor systems experience a natal kick when the stars transition to white dwarfs, neutron stars, or black holes. The kick velocity can be up to several hundreds of kilometers per second (Fryer & Kalogera 1997; Fryer et al. 1998)—potentially larger than the escape velocity of its host galaxy, which could expel the progenitor system and result in a large offset from the host galaxy.

However, SSS17a has a relatively small offset compared to the typical offsets of sGRBs. Combined with its likely old age, the location close to the center of the host galaxy suggests that the progenitor system of SSS17a was bound to NGC 4993. Assuming a stellar mass of $\log(M/M_{\odot}) = 10.49$ (Section 3.1), the escape velocity of NGC 4993 is 350 km s^{-1} at the transient location. We therefore have a constraint on the SSS17a progenitor system kick of $\leqslant$350 km s^{-1}, which is consistent with the kicks seen for Milky Way neutron star binaries (Fryer & Kalogera 1997; Wang et al. 2006; Wong et al. 2010).

Assuming the distance to the nearest likely globular cluster (290 pc; see Section 3.5) and the age of the youngest stellar population (2.8 Gyr; see Section 3.2), a velocity of $\sim$0.1 km s^{-1} is sufficient for the progenitor to travel from a globular cluster to its the current location. Thus, the progenitor kick should be dominated by the escape velocity of the globular cluster (typically several tens of kilometers per second), which makes it hard to exclude the possibility that the progenitor originated in a globular cluster.

5. Conclusions

In this work, we investigate the host environment of SSS17a, the first electromagnetic counterpart to a gravitational-wave source. We use optical spectroscopy and broadband UV-through-IR photometry of the host galaxy to constrain the host properties, such as stellar mass, SFR, age, and metallicity. Below we summarize our main findings.

1. NGC 4993, the host galaxy of SSS17a, is an S0 galaxy at 40 Mpc. It is massive and shows negligible recent star formation. Its mean stellar age is high, suggesting that the progenitor system likely originated from an old stellar population (an age of >2.8 Gyr). NGC 4993 is similar to galaxies that have hosted sGRBs and the expected host galaxies of BNS mergers. It is unlike typical host galaxies for other transient classes, being the most distinct from long GRB host galaxies.

2. Its small projected offset combined with its likely old age suggests that the progenitor system of SSS17a was gravitationally bound to NGC 4993. This then implies a limit on the kick velocity of the progenitor system that is $\leqslant$350 km s^{-1}.

3. Many likely globular clusters are detected in the host galaxy, including close to the position of SSS17a. We cannot exclude the possibility that the progenitor of SSS17a originated from a globular cluster.

The galactic environment of SSS17a provides additional constraints on its progenitor system beyond that extracted from the GW data and the EM observations of SSS17a itself. With larger samples of BNS merger host galaxies, we will be able to determine if they differ in any way from sGRB host galaxies.

ORCID iDs

D. A. Coulter ⓘ https://orcid.org/0000-0003-4263-2228
A. L. Piro ⓘ https://orcid.org/0000-0001-6806-0673
J. X. Prochaska ⓘ https://orcid.org/0000-0002-7738-6875
E. Ramirez-Ruiz ⓘ https://orcid.org/0000-0003-2558-3102
B. J. Shappee ⓘ https://orcid.org/0000-0003-4631-1149

References

Avila, R. J., Hack, W., Cara, M., et al. 2015, in ASP Conf. Ser. 495, Astronomical Data Analysis Software and Systems XXIV, ed. A. R. Taylor & E. Rosolowsky (San Francisco, CA: ASP), 281
Behroozi, P. S., Ramirez-Ruiz, E., & Fryer, C. L. 2014, ApJ, 792, 123
Berger, E. 2014, ARA&A, 52, 43
Bertin, E., & Arnouts, S. 1996, A&AS, 117, 393
Bianchi, L., Shiao, B., & Thilker, D. 2017, ApJS, 230, 24
Bloom, J. S., Kulkarni, S. R., & Djorgovski, S. G. 2002, AJ, 123, 1111
Capaccioli, M., Spavone, M., Grado, A., et al. 2015, A&A, 581, A10
Cappellari, M., & Emsellem, E. 2004, PASP, 116, 138
Cardelli, J. A., Clayton, G. C., & Mathis, J. S. 1989, ApJ, 345, 245
Chambers, K. C., Magnier, E. A., Metcalfe, N., et al. 2016, arXiv:1612.05560
Coulter, D. A., Foley, R. J., Kilpatrick, C. D., et al. 2017, Sci, https://doi.org/science.aaq9811
de Vaucouleurs, G., de Vaucouleurs, A., Corwin, H. G., Jr., et al. 1991, Third Reference Catalogue of Bright Galaxies, Vol. II, III (New York: Springer)
Dressler, A., Bigelow, B., Hare, T., et al. 2011, PASP, 123, 288
Dressler, A., Hare, T., Bigelow, B. C., & Osip, D. J. 2006, Proc. SPIE, 6269, 62690F
Eichler, D., Livio, M., Piran, T., & Schramm, D. N. 1989, Natur, 340, 126
Faifer, F. R., Forte, J. C., Norris, M. A., et al. 2011, MNRAS, 416, 155
Fioc, M., & Rocca-Volmerange, B. 1997, A&A, 326, 950
Fong, W., Berger, E., Chornock, R., et al. 2013, ApJ, 769, 56
Freedman, W. L., Madore, B. F., Gibson, B. K., et al. 2001, ApJ, 553, 47
Fruchter, A. S., Levan, A. J., Strolger, L., et al. 2006, Natur, 441, 463
Fryer, C., Burrows, A., & Benz, W. 1998, ApJ, 496, 333
Fryer, C., & Kalogera, V. 1997, ApJ, 489, 244
Grindlay, J., Portegies Zwart, S., & McMillan, S. 2006, NatPh, 2, 116
Harris, W. E., Harris, G. L., & Hudson, M. J. 2015, ApJ, 806, 36
HST 2017, GCN, 21536
INTEGRAL 2017, GCN, 21507
Kelly, P. L., & Kirshner, R. P. 2012, ApJ, 759, 107
Kennicutt, R. C., Jr. 1998, ARA&A, 36, 189
Le Borgne, D., & Rocca-Volmerange, B. 2002, A&A, 386, 446
Lee, W. H., & Ramirez-Ruiz, E. 2007, NJPh, 9, 17
Lee, W. H., Ramirez-Ruiz, E., & van de Ven, G. 2010, ApJ, 720, 953
Leibler, C. N., & Berger, E. 2010, ApJ, 725, 1202
LIGO/Virgo Collaboration 2017a, GCN, 21505
LIGO/Virgo Collaboration 2017b, GCN, 21509
Magnier, E. A., Schlafly, E. F., Finkbeiner, D. P., et al. 2016, arXiv:1612.05242
Makarov, D., & Karachentsev, I. 2011, MNRAS, 412, 2498
One-Meter Two-Hemisphere (1M2H) Collaboration 2017, GCN, 21529
Pan, Y.-C., Sullivan, M., Maguire, K., et al. 2014, MNRAS, 438, 1391
Peng, C. Y., Ho, L. C., Impey, C. D., & Rix, H.-W. 2002, AJ, 124, 266
Peng, E. W., Jordán, A., Côté, P., et al. 2008, ApJ, 681, 197
Prieto, J. L., Stanek, K. Z., & Beacom, J. F. 2008, ApJ, 673, 999
Prochaska, J. X., Bloom, J. S., Chen, H.-W., et al. 2006, ApJ, 642, 989
Salpeter, E. E. 1955, ApJ, 121, 161
Samsing, J., MacLeod, M., & Ramirez-Ruiz, E. 2014, ApJ, 784, 71
Sánchez-Blázquez, P., Peletier, R. F., Jiménez-Vicente, J., et al. 2006, MNRAS, 371, 703
Sarzi, M., Falcón-Barroso, J., Davies, R. L., et al. 2006, MNRAS, 366, 1151
Schlafly, E. F., & Finkbeiner, D. P. 2011, ApJ, 737, 103
Shabala, S. S., Ting, Y.-S., Kaviraj, S., et al. 2012, MNRAS, 423, 59
Shappee, B. J., Simon, J. D., Drout, M. R., et al. 2017, Sci, https://doi.org/science.aaq0186/science.aaq0186
Skrutskie, M. F., Cutri, R. M., Stiening, R., et al. 2006, AJ, 131, 1163
Spitler, L. R., & Forbes, D. A. 2009, MNRAS, 392, L1
Svensson, K. M., Levan, A. J., Tanvir, N. R., Fruchter, A. S., & Strolger, L.-G. 2010, MNRAS, 405, 57
VAST 2017, GCN, 21645
Vazdekis, A., Sánchez-Blázquez, P., Falcón-Barroso, J., et al. 2010, MNRAS, 404, 1639
Wang, C., Lai, D., & Han, J. L. 2006, ApJ, 639, 1007
Wang, X., Wang, L., Filippenko, A. V., Zhang, T., & Zhao, X. 2013, Sci, 340, 170
Wong, T.-W., Willems, B., & Kalogera, V. 2010, ApJ, 721, 1689
Wright, E. L., Eisenhardt, P. R. M., Mainzer, A. K., et al. 2010, AJ, 140, 1868
Yang, X., Mo, H. J., & van den Bosch, F. C. 2008, ApJ, 676, 248
Zheng, Z., & Ramirez-Ruiz, E. 2007, ApJ, 665, 1220